State-resolved mutual neutralization of $^{16}O^+$ with $^1H^-$ and $^2H^-$ at collision energies below 100 meV

Alice F. Schmidt-May [1,*] Paul S. Barklem [2] Jon Grumer [2] Anish M. Amarsi [2] Mikael Björkhage [1] Mikael Blom [1]
Arnaud Dochain [1] MingChao Ji [1] Paul Martini [1] Peter Reinhed [1] Stefan Rosén [1] Ansgar Simonsson [1]
Henning Zettergren [1] Henrik Cederquist [1] and Henning T. Schmidt [1,†]

[1]*Department of Physics, Stockholm University, Stockholm 10691, Sweden*
[2]*Theoretical Astrophysics, Department of Physics and Astronomy, Uppsala University, Uppsala 75237, Sweden*

We measured the product-state distribution and its dependence on the hydrogen isotope for the mutual neutralization between $^{16}O^+$ and $^{1,2}H^-$ at the double electrostatic ion-beam storage ring DESIREE for center-of-mass collision energies below 100 meV. We find at least six product channels into ground-state hydrogen and oxygen in different excited states. The majority of oxygen products populate terms corresponding to $2s^2\,2p^3(^4S^\circ)4s$ with $^5S^\circ$ as the main reaction product. We also observe product channels into terms corresponding to $2s^2\,2p^3(^4S)3p$. Collisions with the heavier hydrogen isotope yield a branching into these lower excited states smaller than collisions with $^1H^-$. The observed reaction products agree with the theoretical predictions. The detailed branching fractions, however, differ between the theoretical results, and none of them fully agree with the experiment.

I. INTRODUCTION

Oxygen is the third most abundant element in the Universe after hydrogen and helium, and its properties and interactions are important to understand in order to be able to form a correct picture of the chemistry and physics of many astrophysical environments [1]. As a dominant source of opacity and as a catalyst in the CNO cycle, oxygen has a key role in stellar structure and evolution [2]. Oxygen is also an important tracer of the evolution of galaxies [3,4], as well as of the properties of exoplanets [5].

In particular, the solar oxygen abundance is currently the subject of debate [6]. Improved stellar spectra modeling based on three-dimensional radiation hydrodynamics and including departures from local thermodynamic equilibrium (LTE) have resulted in a significant downwards revision of the oxygen abundance in the Sun, as well as of other abundant light elements including carbon and nitrogen [7–9]. The corresponding reduction in opacity, however, results in significant discrepancies between standard models of the Sun and precise helioseismic measurements [10]. The origin of these discrepancies remains unclear [11], but one possibility is that the oxygen abundance derived from the stellar spectrum is in error. The three O I absorption lines at 777 nm are the strongest

feature at visible and near infrared wavelengths and have been the subject of intensive investigations [12–17]. This triplet is highly sensitive to deviations from LTE. Thus, accurate oxygen abundances require collisional-radiative modeling to solve for the more general state of statistical equilibrium. This in turn requires a complete description of the most important inelastic collision processes.

The cross sections for inelastic collisions between oxygen and hydrogen pose some of the largest uncertainties for gauging the oxygen abundance in the Sun and solar-type stars [13]. Different theoretical models lead to vastly different conclusions [15,17]. One theoretical set of cross sections were obtained via a linear-combination-of-atomic-orbitals (LCAO) approach with the multichannel Landau-Zener formula [18,19] for the electron transfer mechanism, supplemented with data for a momentum transfer mechanism following the free-electron model in the impulse approximation of Kaulakys [20,21], labeled LCAO + impulse by Amarsi *et al.* [17]. Another theoretical approach, also tested by Bergemann *et al.* [15] and referred to as the quantum hopping probability current (QPC), used multireference configuration-interaction potentials by Mitrushchenkov *et al.* [22] to calculate cross sections within a Landau-Zener scheme [23]. In the original QPC publication [23], excitations in the neutral oxygen product higher than 12 eV were omitted, but higher excited states were included for the study by Bergemann *et al.* [15].

There is some astrophysical evidence to support the LCAO + impulse model, in that it reproduces the variation of the O I 777-nm triplet over the solar disk [15–17] and suggests oxygen abundances consistent with those from other diagnostics [9]. Indeed, Bergemann *et al.* [15] and the follow-up study of Pietrow *et al.* [16], following Amarsi *et al.* [17], base their final oxygen abundance on the LCAO + impulse
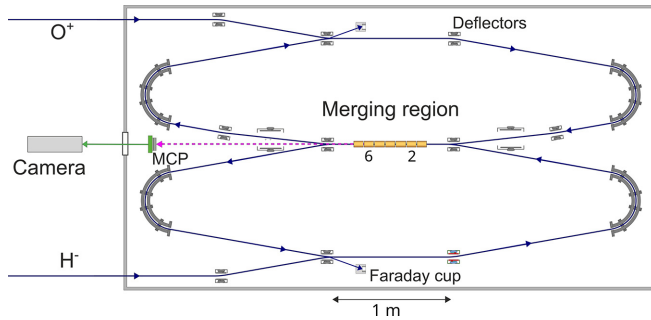
FIG. 1. Schematic of the parts of DESIREE most relevant for the present study. The ion trajectories are depicted in dark blue, the neutral reaction products in pink, and the light from the phosphor screen anode in green. The drift tubes in the merging region are shown in gold and the ones biased in the experiment were no. 2 for $^2H^-$, and no. 6 for $^1H^-$. For details of the setup, see Refs. [25,26].

approach. There is a risk, however, that this agreement is coincidental and that errors in the theoretical collision cross sections are compensated for by other errors in the spectrum modeling.

Consequently, experimental investigations on the inelastic collisions between oxygen and hydrogen are of high relevance to astrophysics, particularly at the subelectronvolt collision energies of stellar photospheres. Mutual neutralization is a useful tool to test the general theoretical description of the electron transfer mechanism as the nonadiabatic coupling between ionic and neutral states, central to mutual neutralization, also governs the inelasticity of neutral-neutral collisions by electron transfer. Previous experimental results on mutual neutralization between $^{16}O^+$ and $^2H^-$ [24] at millielectronvolt collision energies did not report population in the neutral oxygen terms corresponding to $2s^2 2p^3(^4S°)3p$ which are predicted to be significantly populated based on theoretical calculations [15,19]. In particular, Amarsi *et al.* [17] found the population of $2s^2 2p^3(^4S°)3p\ ^5P$ to be of relevance in the oxygen abundance analysis of the Sun [17]. Here, we present an experimental study of mutual neutralization reactions at subelectronvolt collision energies of $^{16}O^+$ with $^2H^-$ and $^1H^-$ and compare it to the two theoretical calculations that have been used to extract information about the amount of oxygen in the Sun.

II. EXPERIMENT

The experiments were performed at DESIREE, the cryogenic double electrostatic ion-beam storage ring facility in Stockholm which has been described in detail before (see, e.g., Refs. [25,27]). A schematic of the experimental setup is presented in Fig. 1. The first description of the experimental procedure for mutual neutralization experiments at DESIREE can be found in Ref. [26]. Contrary to most of the earlier mutual neutralization experiments at DESIREE, however, the present experiments were undertaken in single-pass, continuous-beam mode, as described by Schmidt-May *et al.* [28].

The $^{1,2}H^-$ ions were produced in a Source of Negative Ions by Cesium Sputtering (SNICS) [29] using TiH_2 in a

copper cathode and accelerated by a potential difference of −6 and −7.8 kV for $^1H^-$ and $^2H^-$, respectively. An electron cyclotron resonance ion source (Monogan M-100 ECRIS, Pantechnik, Bayeux, France) was used to produce the oxygen cations. After ionization by electron impact at 60 eV, which is similar to the ionization mechanisms in the ECRIS, Hughes and Tiernan [30] found metastable fractions in $^{16}O^+$ between 4% when produced from carbon dioxide and up to 90% when produced from water. We ran the experiment with $^{16}O^+$ ions from molecular oxygen, carbon dioxide, and water vapor to test for contributions of the long-lived first excited states ^2D and ^2P in $^{16}O^+$. We did not find any contribution from metastables, and the branching fractions published here stem from $^{16}O^+$ produced from carbon dioxide in the ECRIS. The potential difference to accelerate the $^{16}O^+$ ion beam was set to 86 kV for collisions with $^1H^-$ and to 56 kV for collisions with $^2H^-$.

The ions were mass selected and guided into the storage ring, where the two ion beams were overlapped in the merging region (see Fig. 1). There, a selection of seven drift tubes can be biased to match the velocities of the anionic and cationic beams and to reach subelectronvolt center-of-mass collision energies. The drift-tube voltage that matches the velocities was found by searching for the setting at which the probabilities for the hydrogen atom and the oxygen atom to arrive first or second at the detector were the same. We biased a 7.6-cm-long drift tube with its center 1.85 m from the detector at −680 V when measuring mutual neutralization of $^{16}O^+$ + $^2H^-$ (see Fig. 1). For $^{16}O^+$ + $^1H^-$, we biased a 7.6-cm-long drift tube at −560 V, centered 1.52 m from the detector.

The ions were guided onto their ring trajectories after the merging region and collected by a Faraday cup. The neutrals that are produced in mutual neutralization in the merging region are not deflected and arrived nearly at the same time at the detector. The inner-chamber part of the detection system consists of a Z-stack of three microchannelplates with a 75-mm diameter and a phosphor-screen anode behind them. The light from the phosphor is viewed from outside the vacuum chambers by a TPX3CAM camera [31] of Amsterdam Scientific Instruments [32] through vacuum-chamber view ports. The simultaneous detection of time and position of each pixel activation on the 256×256 pixel chip in the camera allows the reliable detection of two, and more, coincident particles [33,34].

Activated pixels were assigned and aggregated to time and position of individual spots utilizing the clustering algorithm DBSCAN [35,36] inspired by Al-Refaie *et al.* [37]. As the time-of-activation of a pixel is dependent on the intensity of the light pulse [38], an intensity-dependent correction was applied to the registered time of arrival. We established the temporal delay specific to each intensity in a separate setup for calibration using individual detector events by splitting the light pulse from the phosphor screen and measuring the temporal offset between a photomultiplier tube signal and the registered time-of-arrival on the TPX3CAM.

Two detection events are considered to result from a single mutual neutralization event in the biased region when their arrival times are less than 50 ns apart and more than 200 ns apart from the previous and following events.

III. ANALYSIS

The analysis mainly follows the description given in Refs. [26,39]. By combining the measured arrival-time difference and positions, a three-dimensional vector between the two neutrals when their center-of-mass crosses the detector plane is obtained. Its magnitude, the product separation r, is related to the total kinetic energy E, after the mutual neutralization reaction, in the center-of-mass system via

$$r = \frac{L}{v}\sqrt{2\frac{E}{\mu}}, \tag{1}$$

with v being the velocity of the center-of-mass in the laboratory frame of reference and μ the reduced mass of the diatomic system. Further, L is the distance from the position of the mutual neutralization reaction to the detector and its average is equal to the distance between the center of the biased section and the detector. E is the sum of the product-channel-specific kinetic energy release (KER) of the reaction and the center-of-mass collision energy.

We exclude mutual neutralization events with a $\cos\theta \geqslant 0.2$, with θ being the polar angle of the product-separation vector with respect to the beam axis. This is an efficient discrimination against mutual neutralization events occurring in the fringe fields of the biased region, which have larger arrival-time differences due to the unmatched ion beam velocities. Additionally, the high ion beam speeds needed for light ions cause very small arrival-time differences which are at most 10 times larger than the least significant bit of the TPX3CAM time stamp of 1.56 ns [40]. Thus, excluding events for which the product separation is dominated by the arrival-time difference increases the resolution in the product separation distribution. The $\cos\theta$ distributions of all channels are isotropic at low collision energies and, without a channel-dependent anisotropy, cuts in $\cos\theta$ have no influence on the extracted branching fractions.

To deduce branching fractions, the product separation distributions are fitted with a linear combination of model functions, one per product channel. The model function is a convolution of the distribution resulting from the simulated potential in the merging section, which depends on the length of the biased drift-tube region, with a Lorentzian function accounting for any broadening, e.g., velocity spreads and detection imprecision. Additional to a scaling factor for each channel, the fitting parameters include a common width of the Lorentzian for all peaks and a common energy offset corresponding to the most probable center-of-mass collision energy in the biased region. The most-probable collision energy can be elevated due to multiple factors, e.g., a mismatch of the ion beams' velocities, a small angle between the ion beams and most likely dominantly by the ion beams' divergence. The KER of a given product channel is calculated by subtracting the electron affinity of hydrogen and the excited-state energy of oxygen from its ionization energy using tabulated values from the National Institute of Science and Technology (NIST) [41,42].

In the fitting procedure, a distribution of center-of-mass collision energies is formed by the global energy offset and the potential-dependent center-of-mass collision energies and

yields a mean center-of-mass collision energy and its uncertainty. The counting statistical error is taken into account in the optimization and the stated errors of the deduced branching fractions are the propagated standard deviations from fitted scaling parameters.

We ran fits with the energetically accessible product channel $^1\text{H}^-(1s^2) + {}^{16}\text{O}^+(2s^2\,2p^3\ {}^4S^\circ) \rightarrow {}^{1,2}\text{H}\,(2s^1) + \text{O}(2s^2\,2p^4\ {}^1D^\circ)$ that was not included in the theoretical studies. We found no significant population and excluded this channel when we extracted the final branching fractions. Additionally, we do not include product channels with a KER outside the region between 0.5 and 2.7 eV as our measurements do not indicate any population there. The two product channels $^1\text{H}^-(1s^2) + {}^{16}\text{O}^+(2s^2\,2p^3\ {}^4S^\circ) \rightarrow {}^{1,2}\text{H}\,(1s^1) + \text{O}(2s^2\,2p^33d\ {}^5D)$ and $\text{O}(2s^2\,2p^33d\ {}^3D^\circ)$ are less than 1 meV apart and we treat them as one channel, denoted $^{5,3}D^\circ$, in the fitting procedure.

IV. RESULTS

We find significant population in six excited states of oxygen and ground-state hydrogen after the mutual neutralization of $^{16}\text{O}^+ + {}^1\text{H}^-$ at an average center-of-mass collision energy of 36(3) meV [Fig. 2(a)]. The channels correspond to oxygen states with an $2s^2\,2p^3({}^4S^\circ)\ {}^{16}\text{O}^+$ core. For mutual neutralization between $^{16}\text{O}^+ + {}^2\text{H}^-$ at 31(3) meV, we find only four product channels [Fig. 2(b)].

Independent of the hydrogen isotope, more than half of the oxygen products populate terms corresponding to $({}^4S^\circ)4s$. The branching fraction into the $({}^4S^\circ)4s\ {}^5S^\circ$ state alone is measured to be 39(2)% and 47.1(8)% for $^1\text{H}^- + {}^{16}\text{O}^+$ and $^2\text{H}^- + {}^{16}\text{O}^+$, respectively. The branching into the other product channels drops with the difference in energy to this dominant channel. In Table I, our experimental branching fractions and the difference between the results of the two isotopes are presented together with the theoretical predictions based on LCAO [19] and QPC [15]. Figure 2 shows the measured KER distribution together with the best fit and the theoretical predictions folded by the experimental response function.

The $({}^4S^\circ)3p\ {}^3P$ channel has a significant population for both isotopes. The combined branching fraction of $({}^4S^\circ)3p\ {}^3P$ and the neighboring $({}^4S^\circ)3p\ {}^5P$ decreases from 13.4% in $^1\text{H}^- + {}^{16}\text{O}^+$ to 6.0% in $^2\text{H}^- + {}^{16}\text{O}^+$. The branching into the main reaction product and higher excited states $({}^4S^\circ)3d\ {}^5D$ and ^3D, treated as one channel in the analysis, is larger with $^2\text{H}^-$ than with $^1\text{H}^-$ while the population of $({}^4S^\circ)4p\ {}^5P$ is smaller with the heavier isotope.

V. DISCUSSION

Comparing our findings to the theoretical predictions, we notice that both calculations predict the same main reaction products as those seen in the measurements. The calculated branching fractions do not, however, fully match our experimental results. Both calculations predict populations in $({}^4S^\circ)3p\ {}^3P$ and $({}^4S^\circ)3p\ {}^5P$ significantly higher than what we measure. A plausible explanation for this discrepancy is the position of the avoided curve crossings involving these states. As seen in Fig. 3, the nonadiabatic regions of channels corresponding asymptotically to $({}^4S^\circ)3p\ {}^3P$ and $({}^4S^\circ)3p\ {}^5P$

TABLE I. The measured branching fractions (BF) into different states of the neutral oxygen after mutual neutralization with ^{1}H$^-$ and ^{2}H$^-$ at collision energies of 36(3) meV and 31(3) meV, respectively, in comparison with the BF predicted by LCAO [19] and QPC [15] calculations. Unless stated otherwise, the hydrogen is in its ground state. The calculated BF have no significant dependence on the center-of-mass collision energy at collision energies below 500 meV and the specific calculated BF were taking at 40 and 33 meV, for QPC and LCAO respectively. The three last columns show the measured and predicted difference between ^{1}H$^-$ and ^{2}H$^-$. Stated uncertainties stem from the least-square fitting procedure taking counting statistics into account but do not include a potentially erroneous shape of the model function, describing the experimental response function. This could lead to a systematic error of up to 1%.

Electronic state of oxygen			BF with ^{1}H (%)			BF with ^{2}H(%)		Isotope difference (%pt.)	
Configuration	Term	KER (eV)	Expt.	LCAO	QPC	Expt.	LCAO	Expt.	LCAO
$2s^2 2p^4$	^3P +H ($n=2$)	2.67	< 1%	3×10^{-4}	2.0	< 1%	1×10^{-4}		-2×10^{-4}
$2s^2 2p^3(^4S^\circ)3p$	^5P	2.13	0.9(3)	2.9	1.1	< 1%	1.0	−0.8(4)	−1.9
$2s^2 2p^3(^4S^\circ)3p$	^3P	1.88	12.5(8)	21.2	17.4	5.9(4)	14.5	−6.6(9)	−6.7
$2s^2 2p^3(^4S^\circ)4s$	$^5S^\circ$	1.04	39(2)	42.6	33.0	47.1(8)	51.1	8(3)	8.5
$2s^2 2p^3(^4S^\circ)4s$	$^3S^\circ$	0.94	26(2)	18.5	9.0	26.8(8)	18.2	−1(3)	−0.2
$2s^2 2p^3(^4S^\circ)3d$	$^{5,3}D^\circ$	0.79	19(1)	14.2	36.8	19.4(6)	14.5	0(2)	0.3
$2s^2 2p^4$	^1D +H ($n=2$)	0.70	< 1%	—	—	<1%	—		
$2s^2 2p^3(^4S^\circ)4p$	^5P	0.59	1.5(4)	0.6	0.3	<1%	0.7	−1.3(5)	0.1
$2s^2 2p^3(^4S^\circ)4p$	^3P	0.51	< 1%	0.05	0.07	<1%	0.05		0

overlap. This type of situation is not well described in the Landau-Zener model, which assumes that curve crossings are well-separated and that only two states interact at any given internuclear separation.

A noticeable difference between the two calculations is the distribution of reaction products within the higher excited states with KER of 1 eV and below. Here, the LCAO calculations [19] match our experimental result better than the QPC calculations [15]. QPC predicts a branching fraction into $(^4S^\circ)3d$ higher than that into $(^4S^\circ)4s$ ^5S, and the $(^4S^\circ)4s$ ^3S population is calculated to be less than half of what we measure. As both calculations use a Landau-Zener scheme for the dynamics, the discrepancy between the two models most probably stems from the different description of the electronic structure of the OH quasimolecule formed during the collision and any resulting difference in potentials and couplings.

In addition, the LCAO [19] and QPC [15] results differ in the expected excitation of the electron donor, hydrogen, with oxygen in its ground state. This product channel implies a simultaneous rearrangement of two electrons, and in the LCAO calculations that we are comparing to here, this channel was included with an estimate of the relevant two-electron coupling strength. The LCAO branching fraction calculated by these means is, however, very close to 0, whereas the QPC branching fraction is 2.0% for ^{16}O$^+$ + ^{1}H$^-$. Our experimental results do not exclude a small population below 1%, but show no peak at the expected position.

The isotope effect in the form of differences in the product distributions for ^{16}O$^+$ colliding with ^{1}H$^-$ or ^{2}H$^-$ is found to be slightly weaker in the experimental than in the LCAO [19] results, but the general trend of the smaller population in the lower excited states with the heavier isotope is in line with our experimental findings. A smaller population in lower excited states with a heavier hydrogen is consistent with previous observations and analytically derived predictions [28,43].

Amarsi *et al.* [17] found the most important inelastic collision process for forming the O I 777-nm triplet in stellar spectra to be $(^4S^\circ)3s$ $^5S \rightleftharpoons (^4S^\circ)3p$ ^5P transitions in oxygen,

driven by collisions with neutral hydrogen. In the LCAO + impulse model used in that work (see Sec. I), this transition is completely dominated by the momentum transfer mechanism described by the free-electron impulse approximation model. The contribution from this mechanism is about 6 orders of magnitude larger than the contribution from electron transfer via avoided ionic crossings from the LCAO model. For such a transition to occur via the electron transfer mechanism, nonadiabatic transitions are required at two avoided crossings, those corresponding to $(^4S^\circ)3s$ ^5S and $(^4S^\circ)3p$ ^5P states. The measurement for mutual neutralization into $(^4S^\circ)3p$ ^5P probes the electron transfer via the relevant avoided crossing and for ^{1}H the branching fraction is found to be a factor of 3 lower than predicted by LCAO. As discussed earlier, this discrepancy may partly be due to the overlapping of the $(^4S^\circ)3p$ ^5P and $(^4S^\circ)3p$ ^3P avoided crossings. The magnitude and direction of this difference do not suggest that the LCAO modeling of the transition probabilities at the avoided crossing with $(^4S^\circ)3p$ ^5P is in error to such a degree that the conclusion from Ref. [17], that the electron transfer contribution to this transition is negligible in stellar spectral modeling, would be changed.

VI. CONCLUSIONS

We report experimental mutual neutralization studies of ^{1,2}H$^-$ + ^{16}O$^+$ at the double electrostatic ion-beam-storage ring DESIREE. The ions' mass ratio is close to the estimated mass ratio limit of DESIREE [27] for merged-beam ion-ion collision experiments at low energies and the study reported here is one of few subelectronvolt merged-beam experiments with the lightest hydrogen anion ^{1}H$^-$.

Our product separation distributions are only partially state resolved, but by fitting model functions to the measured distribution, we are able to extract branching fractions at center-of-mass collision energies of 36(3) and 31(3) meV for ^{16}O$^+$ + ^{1}H$^-$ and ^{16}O$^+$ + ^{2}H$^-$, respectively. We find that the ground-state ions neutralize into at least six different
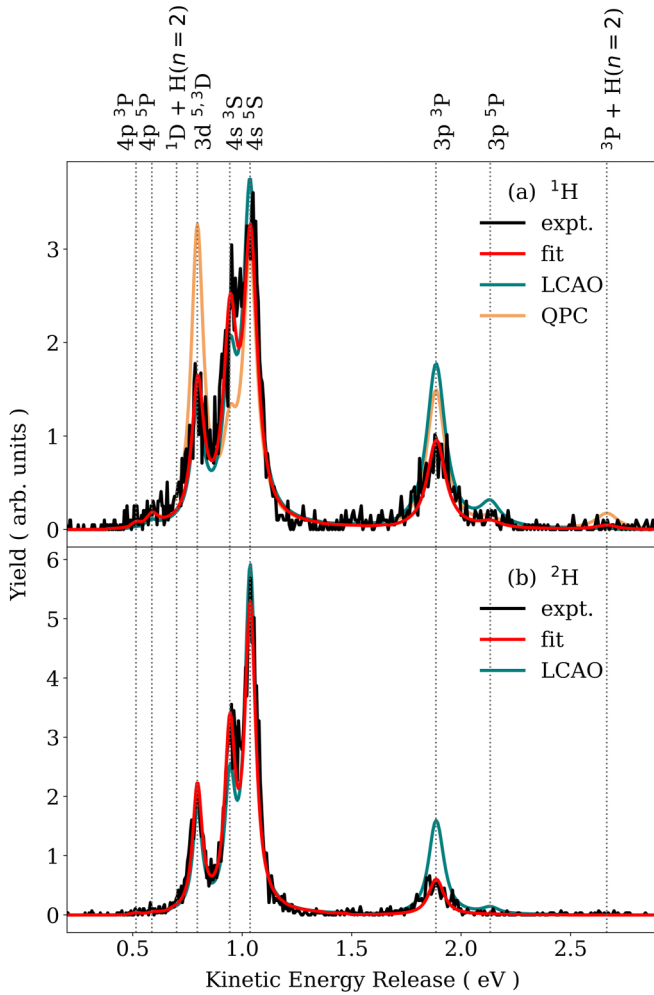
FIG. 2. The measured product separation distributions (black) of $^{16}O^+ + \ ^1H^-$ (a) and $^{16}O^+ + \ ^2H^-$ (b) converted into KER spectra using Eq. (1) and the collision energy obtained by the fit. Only mutual neutralization events with $\cos\theta < 0.2$ are included to show the achievable resolution. The fits to the experimental data as described in Sec. III are displayed in red (medium dark gray), and modeled curves using the fit results for the energetic offset and width with the theoretical calculated branching fractions via QPC [15] are displayed in orange (lightest gray) and via LCAO [19] in teal (darker gray). All curves are normalized to an area of 1. Labels refer to the configuration of the oxygen product with hydrogen in the ground state unless stated otherwise.

FIG. 3. Adabiatic potential energy curves for the $^{16}O\ ^1H$ quasi-molecule in the $^4\Sigma^+$ symmetry calculated with a method based on LCAO [19]. The states are labeled by the states of the oxygen atom in the asymptotic limit with hydrogen in its ground state unless otherwise indicated. The unlabeled, dark blue curve at the top corresponds to $4p\ ^3P$ and the highest state corresponds asymptotically to the ionic state $^{16}O^+ + \ ^1H^-$. Note the logarithmic horizontal axis.

states of oxygen and ground-state hydrogen. More than 60% of all products populate $(^4S°)4s$. The $(^4S°)3p\ ^3P$ term has a significant population for both isotopes, unobserved in earlier experiments [24].

Both QPC [15] and LCAO [19] calculations overestimate the population in $(^4S°)3p\ ^3P$ compared to our experimental value. While there are differences between the experimental results and both theoretical predictions, we find a better agreement with the LCAO calculations [19] for the higher excited oxygen states corresponding to kinetic energy releases between 0.7 and 1.1 eV. In this region, the Landau-Zener approximation is expected to be well fulfilled and the quality of the calculated branching fractions is governed by the
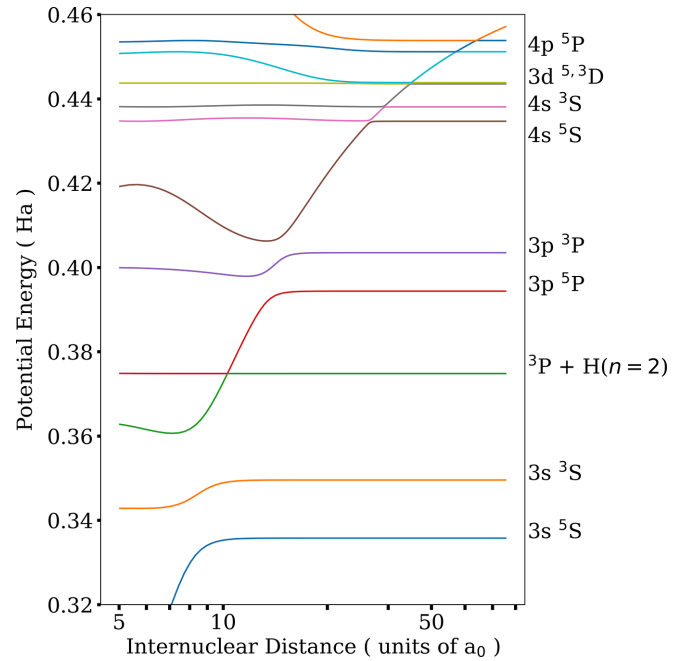
potentials and their couplings at the ionic crossings. With the heavier isotope, we see in the experiment that the population shifts from $(^4S°)3p$ to $(^4S°)4s$, which agrees with the trend predicted by the LCAO calculations.

Overall, the LCAO results [19] reproduce the main features of our measured kinetic energy release distributions in $^{16}O^+ + \ ^{1,2}H^-$ mutual neutralization processes. Given that the electron transfer mechanism in neutral-neutral collisions is governed by the same potentials and couplings, we expect that LCAO describes inelastic processes through electron transfer in neutrals equally well and that the contribution from the electron transfer mechanism to excitation processes in $^{16}O + \ ^{1,2}H$ collisions predicted by LCAO is not drastically in error. The solar modeling and comparison to observations in Refs. [15,17] implies an excitation rate for transitions important to the O I absorption lines at 777 nm that is 6 orders of magnitude larger than expected from LCAO as discussed briefly in Sec. V and in more detail in Ref. [17]. Thus, this work supports the conclusion in Ref. [17] that electron transfer processes are not important for the modeling of these lines in the solar spectrum. The variation of the O I 777-nm triplet over the solar disk suggests that a mechanism different from electron transfer could be at play. Whether the impulse approximation model [21,44], or some other model, gives an adequate description of such a mechanism in low-lying states is an open question.

All resulting data shown in the figures are available electronically under a Creative Commons license [45].

[1] D. Romano, The evolution of CNO elements in galaxies, Astron. Astrophys. Rev. **30**, 7 (2022).

[2] D. A. VandenBerg, P. A. Bergbusch, A. Dotter, J. W. Ferguson, G. Michaud, J. Richer, and C. R. Proffitt, Models for metal-poor stars with enhanced abundances of C, N, O, Ne, Na, Mg, Si, S, Ca, and Ti, in turn, at constant helium and iron abundances, Astrophys. J. **755**, 15 (2012).

[3] K. Z. Arellano-Córdova, D. A. Berg, J. Chisholm, P. A. Haro, M. Dickinson, S. L. Finkelstein, F. Leclercq, N. S. J. Rogers, R. C. Simons, E. D. Skillman, J. R. Trump, and J. S. Kartaltepe, A first look at the abundance pattern—O/H, C/O, and Ne/O— in $z > 7$ galaxies with JWST/NIRSpec, Astrophys. J. Lett. **940**, L23 (2022).

[4] M. Chruślińska, R. Pakmor, J. Matthee, and T. Matsuno, Trading oxygen for iron I: the [O/Fe] – specific star formation rate relation of galaxies, arXiv:2308.00023.

[5] M. R. Line, M. Brogi, J. L. Bean, S. Gandhi, J. Zalesky, V. Parmentier, P. Smith, G. N. Mace, M. Mansfield, E. M.-R. Kempton, J. J. Fortney, E. Shkolnik, J. Patience, E. Rauscher, J.-M. Désert, and J. P. Wardenier, A solar C/O and sub-solar metallicity in a hot Jupiter atmosphere, Nature (London) **598**, 580 (2021).

[6] J. Christensen-Dalsgaard, Solar structure and evolution, Living Rev. Sol. Phys. **18**, 2 (2021).

[7] M. Asplund, N. Grevesse, A. J. Sauval, T. G. Barnes, and F. N. Bash, *Cosmic Abundances as Records of Stellar Evolution and Nucleosynthesis* (ASP, San Francisco, CA, 2005), Vol. 336.

[8] M. Asplund, A. Amarsi, and N. Grevesse, The chemical make-up of the Sun: A 2020 vision, Astron. Astrophys. **653**, A141 (2021).

[9] A. M. Amarsi, N. Grevesse, M. Asplund, and R. Collet, The solar carbon, nitrogen, and oxygen abundances from a 3D LTE analysis of molecular lines, Astron. Astrophys. **656**, A113 (2021).

[10] S. Basu and H. Antia, Helioseismology and solar abundances, Phys. Rep. **457**, 217 (2008).

[11] G. Buldgen, P. Eggenberger, A. Noels, R. Scuflaire, A. M. Amarsi, N. Grevesse, and S. Salmonhigher metal abundances do not solve the solar problem, Astron. Astrophys. **669**, L9 (2023).

[12] T. M. D. Pereira, M. Asplund, and D. Kiselman, Oxygen lines in solar granulation - II. Centre-to-limb variation, NLTE line formation, blends, and the solar oxygen abundance, Astron. Astrophys. **508**, 1403 (2009).

[13] M. Steffen, D. Prakapavicius, E. Caffau, H.-G. Ludwig, P. Bonifacio, R. Cayrel, A. Kucinskas, and W. C. Livingston, The photospheric solar oxygen project. IV. 3D-NLTE investigation of the 777 triplet lines, Astron. Astrophys. **583**, A57 (2015).

[14] A. M. Amarsi, M. Asplund, R. Collet, and J. Leenaarts, Non-LTE oxygen line formation in 3D hydrodynamic model stellar atmospheres, Mon. Not. R. Astron. Soc. **455**, 3735 (2016).

[15] M. Bergemann, R. Hoppe, E. Semenova, M. Carlsson, S. A. Yakovleva, Y. V. Voronov, M. Bautista, A. Nemer, A. K. Belyaev, J. Leenaarts, L. Mashonkina, A. Reiners, and M. Ellwarth, Solar oxygen abundance, Mon. Not. R. Astron. Soc. **508**, 2236 (2021).

[16] A. G. M. Pietrow, R. Hoppe, M. Bergemann, and F. Calvo, Solar oxygen abundance using SST/CRISP center-to-limb observations of the O 772 Å line, Astron. Astrophys. **672**, L6 (2023).

[17] A. M. Amarsi, P. S. Barklem, M. Asplund, R. Collet, and O. Zatsarinny, Inelastic O + H collisions and the OI 777 nm solar centre-to-limb variation, Astron. Astrophys. **616**, A89 (2018).

[18] P. S. Barklem, Excitation and charge transfer in low-energy hydrogen-atom collisions with neutral atoms: Theory, comparisons, and application to Ca, Phys. Rev. A **93**, 042705 (2016).

[19] P. S. Barklem, Excitation and charge transfer in low-energy hydrogen atom collisions with neutral oxygen, Astron. Astrophys. **610**, A57 (2018).

[20] B. Kaulakys and V. Svedas, Collisional ionisation of high-Rydberg atoms. diffusive mechanism, J. Phys. B: At. Mol. Phys. **20**, L565 (1987).

[21] B. Kaulakys, Free electron model for collisional angular momentum mixing of high Rydberg atoms, J. Phys. B: At. Mol. Opt. Phys. **24**, L127 (1991).

[22] A. Mitrushchenkov, M. Guitou, A. K. Belyaev, Y. V. Voronov, and N. Feautrier, Inelastic excitation and charge transfer processes for oxygen in collision with H atoms, J. Chem. Phys. **150**, 064312 (2019).

[23] A. K. Belyaev, Y. V. Voronov, A. Mitrushchenkov, M. Guitou, and N. Feautrier, Inelastic processes in oxygen–hydrogen collisions, Mon. Not. R. Astron. Soc. **487**, 5097 (2019).

[24] X. Urbain, N. de Ruette, A. Dochain, T. Launoy, R. Nascimento, M. Kaminska, M. Stockett, J. Loreau, J. Liévin, N. Vaeck, R. Thomas, H. Schmidt, and H. Cederquist, Merged beam studies of mutual neutralization at subthermal collision energies, J. Phys.: Conf. Ser. **1412**, 062009 (2020).

[25] H. T. Schmidt, R. D. Thomas, M. Gatchell, S. Rosén, P. Reinhed, P. Löfgren, L. Brännholm, M. Blom, M. Björkhage, E. Bäckström, J. D. Alexander, S. Leontein, D. Hanstorp, H. Zettergren, L. Liljeby, A. Källberg, A. Simonsson, F. Hellberg, S. Mannervik, M. Larsson *et al.*, First storage of ion beams in the double electrostatic ion-ring experiment: DESIREE, Rev. Sci. Instrum. **84**, 055115 (2013).

[26] G. Eklund, J. Grumer, S. Rosén, M.C. Ji, N. Punnakayathil, A. Källberg, A. Simonsson, R. D. Thomas, M. H. Stockett, P. Reinhed, P. Löfgren, M. Björkhage, M. Blom, P. S.

Barklem, H. Cederquist, H. Zettergren, and H. T. Schmidt, Cryogenic merged-ion-beam experiments in DESIREE: Final-state-resolved mutual neutralization of Li^+ and D^-, Phys. Rev. A **102**, 012823 (2020).

[27] R. D. Thomas, H. T. Schmidt, G. Andler, M. Björkhage, M. Blom, L. Brännholm, E. Bäckström, H. Danared, S. Das, N. Haag, P. Halldén, F. Hellberg, A. I. S. Holm, H. A. B. Johansson, A. Källberg, G. Källersjö, M. Larsson, S. Leontein, L. Liljeby, P. Löfgren *et al.*, The double electrostatic ion ring experiment: A unique cryogenic electrostatic storage ring for merged ion-beams studies, Rev. Sci. Instrum. **82**, 065112 (2011).

[28] A. F. Schmidt-May, S. Rosén, M.C. Ji, G. Eklund, H. Zettergren, H. Cederquist, H. T. Schmidt, P. S. Barklem, and J. Grumer, Observation of an isotope effect in state-selective mutual neutralization of lithium with hydrogen, Phys. Rev. A **108**, 042810 (2023).

[29] U. N. E. Corp., Source of Negative Ions by Cesium Sputtering - SNICSII, https://www.pelletron.com/wp-content/uploads/2017/02/SNICS-v2.pdf, 2017.

[30] B. M. Hughes and T. O. Tiernan, Determination of the abundance of excited O^+ ions in beams produced by electron impact on O_2, CO_2, N_2O, NO_2, and H_2O, J. Chem. Phys. **55**, 3419 (1971).

[31] A. Nomerotski, M. Chekhlov, D. Dolzhenko, R. Glazenborg, B. Farella, M. Keach, R. Mahon, D. Orlov, and P. Svihra, Intensified Tpx3Cam, a fast data-driven optical camera with nanosecond timing resolution for single photon detection in quantum applications, J. Instrum. **18**, C01023 (2023).

[32] Amsterdam Scientific Instruments, Science Park 106, 1098XG Amsterdam, The Netherlands, www.amscins.com.

[33] M. Poline, A. Dochain, S. Rosén, M.C. Ji, P. Reinhed, A. Simonsson, M. Larsson, H. T. Schmidt, H. Zettergren, R. D. Thomas, S. G. Ard, N. S. Shuman, and A. A. Viggiano, Mutual neutralization of NO^+ with O^-, Phys. Rev. Lett. **132**, 023001 (2024).

[34] A. Bogot, M. Poline, M.C. Ji, A. Dochain, A. Simonsson, S. Rosén, H. Zettergren, H. T. Schmidt, R. D. Thomas, and D. Strasser, The mutual neutralization of hydronium and hydroxide, Science **383**, 285 (2024).

[35] M. Ester, H.-P. Kriegel, J. Sander, and X. Xu, A density-based algorithm for discovering clusters in large spatial databases with noise., in *Proceedings of 2nd International Conference on Knowledge and Data Mining*, KDD Vol. 96 (AAAI, Pennsylvania Ave, NW Suite 300 Washington, DC 20004, USA, 1996), pp. 226–231.

[36] F. Pedregosa, G. Varoquaux, A. Gramfort, V. Michel, B. Thirion, O. Grisel, M. Blondel, P. Prettenhofer, R. Weiss, V. Dubourg, J. Vanderplas, A. Passos, D. Cournapeau, M. Brucher, M. Perrot, and E. Duchesnay, Scikit-learn: Machine learning in Python, J. Mach. Learn. Res. **12**, 2825 (2011).

[37] A. Al-Refaie, M. Johny, J. Correa, D. Pennicard, P. Svihra, A. Nomerotski, S. Trippel, and J. Küpper, PymePix: A python library for SPIDR readout of Timepix3, J. Instrum. **14**, P10003, (2019).

[38] D. Turecek, J. Jakubek, and P. Soukup, USB 3.0 readout and time-walk correction method for Timepix3 detector, J. Instrum. **11**, C12065, (2016).

[39] A. F. Schmidt-May, Final-state-resolved mutual neutralization of Li^+ and H^-, Licentiate thesis, Stockholm University, 2022, https://urn.kb.se/resolve?urn=urn:nbn:se:su:diva-205066.

[40] T. Poikela, J. Plosila, T. Westerlund, M. Campbell, M. D. Gaspari, X. Llopart, V. Gromov, R. Kluit, M. van Beuzekom, F. Zappon, V. Zivkovic, C. Brezina, K. Desch, Y. Fu, and A. Kruth, Timepix3: A 65K channel hybrid pixel readout chip with simultaneous ToA/ToT and sparse readout, J. Instrum. **9**, C05013 (2014).

[41] A. Kramida, Y. Ralchenko, J. Reader, and NIST ASD Team, NIST Atomic Spectra Database (ver. 5.11), available at https://physics.nist.gov/asd, National Institute of Standards and Technology, Gaithersburg, MD, 2021.

[42] R. C. Shiell, X. Hu, Q. J. Hu, and J. W. Hepburn, Threshold ion-pair production spectroscopy (TIPPS) of H_2 and D_2, Faraday Discuss. **115**, 331 (2000).

[43] A. Dochain, V. M. Andrianarijaona, and X. Urbain, Isotope effect for the mutual neutralization reaction at low collision energies: $He^+ + H^-$, Phys. Rev. A **108**, 042809 (2023).

[44] B. Kaulakys, Free electron model for inelastic collisions between neutral atomic particles and Rydberg atoms, Zh. Eksp. Teor. Fiz. **91**, 391 (1986).

[45] The data are available (after publication) at the following repository, http://dx.doi.org/10.5281/zenodo.10823152.